Circular RNA profiling identifies *circ5078* as a *BMPR2*-derived regulator of endothelial translation

M. Martin VandenBroek, BSc[1], Mackenzie C. Sharp, BSc[2], Patrick Thompson[3], Emmanuel Fagbola[1], Douglas Quilty[3], Jeffrey D. Mewburn[1], Anne L. Theilmann, MSc[3], Stephen L. Archer, MD[1], Neil Renwick, MD, PhD[4], Mark L. Ormiston, PhD[1,3]

1. Queen's University Department of Medicine, Kingston, Canada
2. Queen's University School of Computing, Kingston, Canada
3. Queen's University Departments of Biomedical and Molecular Sciences and Surgery, Kingston, Canada
4. Queen's University Department of Pathology and Molecular Medicine, Kingston, Canada

Running Title: *BMPR2* circRNA regulates endothelial translation

Word Count: 6044

Corresponding Author:

Mark L. Ormiston

Queen's University, Departments of

Biomedical and Molecular Sciences,

Medicine and Surgery

Room A209, Botterell Hall

18 Stuart Street

Kingston, Ontario

K7L 3N6, Canada

Tel: 613-533-6241

Email: mark.ormiston@queensu.ca

Abstract

Germline loss-of-function *BMPR2* mutations are the leading genetic cause of pulmonary arterial hypertension (PAH) and are strongly linked to aberrant endothelial proliferation and impaired translational stress responses. While these effects are generally attributed to a loss of the type-II bone morphogenetic protein receptor (BMPR-II), we used circular RNA profiling to identify *circ5078*, a *BMPR2*-derived circular RNA that regulates endothelial translation and cellular phenotype. *circ5078* and linear *BMPR2* mRNA exert opposing effects on endothelial proliferation and stress granule formation, while influencing the translational efficiency of multiple genes by regulating ribosome assembly and translational initiation. In PAH patient-derived endothelial cells lacking linear *BMPR2* mRNA, *circ5078* depletion rescued impaired translational stress responses by rebalancing circular to linear transcript levels, independent of BMPR-II protein. By identifying *circ5078* as a functional *BMPR2* gene product, this work reveals interdependent roles for both linear and circular *BMPR2* transcripts as regulators endothelial translation and proliferation.

Key Words: *BMPR2*, endothelial, circular RNA, proliferation, Caprin-1, translation, stress granule

Introduction

The *BMPR2* gene encodes the bone morphogenetic protein (BMP) type-II receptor (BMPR-II) of the transforming growth factor-β (TGFβ) superfamily. *BMPR2* is expressed ubiquitously throughout the body, including the pulmonary endothelium, where heterozygous loss of function mutations in *BMPR2* have been linked to pulmonary arterial hypertension (PAH), a disease of occlusive pulmonary vascular remodelling[1]. Endothelial *BMPR2* loss is associated with excessive proliferation, enhanced susceptibility to apoptosis, and an impairment of stress-induced translational repression that enables a pro-inflammatory cellular phenotype[2-5].

BMPR2 mutations account for 70% of the heritable form of PAH, and 20% of seemingly idiopathic disease[6]. These mutations, which include deletions, insertions and point-mutations across all exons and many noncoding regions of the *BMPR2* gene[7,8], increase the risk of developing PAH by nearly 20,000-fold, from a prevalence of 10-15 per million in the general population[9,10], to roughly 1 in 4 among *BMPR2* mutation carriers[11]. Studies to examine the molecular mechanisms by which *BMPR2* loss influences endothelial function have largely focused on impaired canonical and non-canonical signalling resulting from reduced BMPR-II protein[12-14]. In contrast, the potential for *BMPR2*-derived RNA transcripts to exert direct functional effects on the pulmonary endothelium has not been considered.

Linear *BMPR2* mRNAs exist as either a full-length transcript containing all 13 exons of the gene (*BMPR2a*), or a truncated variant (*BMPR2b*) lacking exon 12, which encodes for a long cytoplasmic tail domain that is unique to BMPR-II among type-II TGFβ superfamily receptors and is not required for receptor kinase activity[15,16]. Beyond these established mRNAs, the potential existence of alternative, non-coding *BMPR2*-derived transcripts, such as circular RNAs

(circRNAs), has received minimal attention. Similarly, the impact of *BMPR2* loss on the expression of other circRNAs in the pulmonary endothelium is completely unknown.

CircRNAs, which lack free 5' or 3' ends, are more resistant to degradation than traditional linear RNAs and influence cell function by a variety of mechanisms. They can code for proteins, or regulate the availability, subcellular localization, and functionality of other RNAs or proteins[17]. As a consequence, these transcripts represent a promising source for novel regulators of fundamental cellular processes in the diseased pulmonary endothelium. Despite this promise, the study of circRNAs is limited by the methods available to both identify and quantify these transcripts in specific cells or tissues. Over 90,000 putative circRNAs have been annotated across the human genome[18]. However, few of these annotations have been validated experimentally and only a fraction of this subset are captured by commercially available circRNA microarrays[19].

Here, we establish a profile of circRNA expression in human pulmonary arterial endothelial cells (HPAECs), with and without *BMPR2* silencing. Using ultra-high depth RNA-sequencing and an unbiased screen of 92,369 known or proposed human circRNAs, we identify two novel circRNAs derived from the *BMPR2* locus. In doing so, we define a previously unappreciated role for both linear and circular *BMPR2* transcripts in the regulation of endothelial translational control via the interaction of these transcripts with the RNA-binding protein, Caprin-1. Together, these studies provide the first complete profile of circRNA expression in the human pulmonary endothelium and offer evidence supporting a new role for *BMPR2*-derived RNAs as functional gene products that regulate endothelial proliferation and stress responses, independent of signaling via the BMPR-II receptor.

Materials and Methods

Cell culture

Unless stated otherwise, HPAECs and blood outgrowth endothelial cells (BOECs) were plated at a density of 21,000 cells/cm^2 and cultured in endothelial growth media (EGM-2) with 2% FBS or EGM-2MV with 10% FBS, respectively (both Lonza, Basel, Switzerland). For inducing quiescence, HPAECs were cultured for 4 hours in endothelial basal medium (EBM-2, Lonza) with 2% FBS. Demographic and mutation data for patient and control BOEC lines can be found in **Table S1.**

siRNA silencing

Cells were treated with either SMARTpool small interfering RNAs (siRNAs) targeting a range of *BMPR2* transcripts, SMARTpool *CAPRIN1* siRNAs, a non-targeting SMARTpool siRNA control, or custom-designed siRNAs targeting individual circular or linear *BMPR2* transcripts (all Horizon Discovery, Waterbeach, UK). The target sequences for custom siRNAs and catalog information for SMARTpool siRNAs are listed in **Table S2**. For siRNA silencing, Cells were cultured in Opti-MEM reduced serum media (ThermoFisher, Waltham, MA) for 3 hours prior to transfection in fresh Opti-MEM containing DharmaFECT 1 transfection reagent (Horizon Discovery) and siRNAs for 4 hours. For studies examining the silencing of a single target (SMARTpool or custom), siRNAs were used at a final concentration of 10 nmol/L. For experiments examining the combined loss of *circ5078* and *CAPRIN1*, 10 nmol/L of each siRNA was used, with non-targeting control siRNA added as needed to bring the final siRNA concentration in all treatment groups to 20 nmol/L.

RNA isolation and sequencing

One day after plating, HPAECs were transfected with SMARTpool *BMPR2* siRNAs or a non-targeting control. The following day, cells were quiesced for 4 hours, after which they were returned to growth media, with or without 1 ng/mL recombinant human BMP9 (R&D Systems, Minneapolis, MN) for an additional 24 hours. Total RNA was isolated using TRIzol RNA Isolation Reagent (ThermoFisher) and purified using Direct-Zol RNA isolation columns (Zymo Research, Irvine, CA) in accordance with the manufacturer's instructions.

Samples were depleted of ribosomal RNA (NEBNext rRNA Depletion Kit (Human/Mouse/Rat), New England Biolabs, Ipswich, MA) and sequenced using an Illumina NovaSeq 6000 at a mean depth of 312 million paired-end reads per sample (624 million total reads per sample). Reads were trimmed and filtered for quality using Trimmomatic[20], and the quality of the remaining reads was assessed using FastQC (https://www.bioinformatics.babraham.ac.uk/projects/fastqc/).

CircRNA-derived reads were quantified using methods previously described[21]. Briefly, a publicly available list of known or proposed circRNA annotations within the human genome (http://circbase.org/)[18] was used to construct a library of unique splice junctions for each annotated circRNA. Junctions were constructed by extracting 80 bases to the left and right of each splice site from the linear genome and reassembling these sequences in the proper backspliced orientation. Reads measuring 101 base pairs in length were aligned to the junction library using Bowtie2[22], with a minimum score setting of -30. Combining all parameters, reads were required to have a minimum overlap of 21 bases on either side of the junction, with a maximum of five mismatched bases across the entire read, in order to be captured. Aligned reads were quantified using featureCounts[23]. Following the filtering of circRNAs for abundance, differential expression

analysis was conducted using DESeq2[24]. Publicly available GEO datasets from HPAECs (GSE118446), mouse endothelial cells (GSE216635), and rat whole lung (GSE159668) were profiled for circular and linear *BMPR2*-derived transcripts using a similar approach, with junction size and alignment parameters adjusted in accordance with the sequencing read length.

qPCR

RNA was reverse transcribed to cDNA using SuperScript IV VILO (ThermoFisher). qPCR analysis was performed using SYBR Green Master mix (Applied Biosystems, Waltham, MA). Relative gene expression was determined using the ΔΔCt method. Primer sequences can be found in **Table S3**. Generic *BMPR2* primers targeted the boundary of exons 6 and 7, which are shared by all linear *BMPR2* transcripts. *BMPR2a* primers targeted the junction between exon 12 (forward) and exon 13 (reverse), while *BMPR2b* primer pairs relied on a forward primer targeting exon 11, and a reverse primer spanning the exon 11/13 splice junction. The amplicon produced by each set of circRNA primers spanned the unique backspliced circRNA junction. As such, circRNA primers align divergently on the linear genome.

RNase R Digestion

Total RNA (1 μg) from untreated HPAECs was digested by 2U of RNase R enzyme (Lucigen, Middleton, WI) in 10 μL reactions containing 1x digestion buffer. Digestions were performed at 37°C for 20 minutes. 5 μL of digestion product was reverse transcribed and analyzed by qPCR as described above. Samples were compared to a no enzyme control to determine the impact of RNase R digestion.

Cell proliferation assays

For proliferation assays, HPAECs were plated at a density of 10,500/cm^2 in 24-well plates and transfected with siRNAs one day after plating. The following day, HPAECs were quiesced for 4 hours before being switched to EGM-2 with 5% FBS at time 0 of the proliferation assay. Cells were trypsinized and counted at 0- and 96-hours, using a hemocytometer and trypan blue staining to determine cell viability. Media was replaced at the 48-hour time point and proliferation was calculated at 96 hours relative to cell number at time 0.

Apoptosis assay

24 hours after siRNA silencing, HPAECs were transferred to quiescence media containing 100 U/mL penicillin, 100 mg/mL streptomycin, and 0.25 mg/mL amphotericin B for 16 hours, followed by an additional 4 hours with or without an apoptotic stimulus of 10 ng/ml TNFα (Peprotech, Cranbury, NJ) and 20 μg/mL cycloheximide (Sigma-Aldrich, St. Louis, MO). Cells were trypsinized and stained with FITC-conjugated annexin-V and propidium iodide (PI, BD Biosciences, Franklin Lakes, NJ) as per the manufacturer's instructions. Apoptotic cells were determined by events deemed positive for annexin-V and negative for PI by flow cytometry.

Protein isolation and immunoblotting

Buffer compositions can be found in **Table S4**. For whole cell lysates, cells were washed with PBS, snap frozen on dry ice and lysed in RIPA buffer. For cell fractionation lysates, cells were washed in PBS containing 100 μg/mL cycloheximide, scrape collected in homogenization buffer,

and passed five times through a 25G needle. Lysates were centrifuged, and the pellet was resuspended in cytoskeletal bound polysome (CBP) buffer, incubated on ice for 30 minutes, and centrifuged again. The pellet was then washed with CBP, resuspended in membrane bound polysome (MBP) buffer, incubated on ice for 10 minutes, centrifuged, and the supernatant removed. Protein concentration was assessed by DC Protein Assay (Bio-Rad, Hercules, CA), as per the manufacturer's instructions.

Whole cell or cell fraction lysates were run on 10-12% SDS-PAGE gels and transferred to Immobilon-FL PVDF membranes (MilliporeSigma, Burlington, MA). Revert 700 total protein staining (LiCOR, Lincoln, NE) was performed following transfer for normalization within each lane. Following destaining, membranes were blocked in 5% BSA in TBS with 1% Tween (TBST, ThermoFisher) and incubated with primary (overnight) and secondary (1 hour) antibodies in 5% BSA in TBST, as detailed in **Table S5**. Membranes were imaged using the Odyssey Clx Infrared Imaging System and analyzed by Image Studio Software (LiCOR).

RNA-Immunoprecipitation

Lysate collection and immunoprecipitation were performed using the Magna RIP immunoprecipitation assay (MilliporeSigma) and 5 μg of rabbit anti-Caprin-1 (Proteintech, Rosemont, IL) or rabbit IgG control, in accordance with the manufacturer's directions. Protein content of input lysates and immunoprecipitation products were analyzed by immunoblotting as described above. *BMPR2* transcripts from both whole cell lysates and the immunoprecipitated RNA products were amplified by PCR using the primers detailed above and analyzed by agarose gel electrophoresis.

RNA-FISH

Cells were plated on 12 mm, collagen-coated coverslips (Electron Microscopy Sciences) within the wells of 24 well plates and stained for Caprin-1 protein and linear *BMPR2* RNA using the ViewRNA Cells Plus Assay Kit (ThermoFisher). For the fixation and permeabilization steps, buffers were refreshed halfway through the recommended incubation period. Blocking and incubations with Caprin-1 primary (Proteintech, 15112-1-AP, 1:500 dilution) and Alexa488 conjugated secondary antibodies were performed with buffers containing RNaseOUT RNase inhibitor (both ThermoFisher). Coverslips were mounted with ProLong Diamond Antifade with DAPI (ThermoFisher) and cells were imaged by Stimulated Emission Depletion (STED) super-resolution imaging using a Leica SP8 confocal microscope (Leica Microsystems Inc., ON).

Polysome analysis

HPAECs were plated in 15cm dishes and treated with siRNAs, as described above. The day following knockdown, cells were treated with 100 μg/mL of cycloheximide (CHX) (Sigma-Aldrich) for 15 minutes at 37°C. Cells were scrape collected in ice cold PBS with 100 μg/mL CHX, pelleted at 1,000g for 5 minutes at 4°C, and lysed in 350μL of polysome lysis buffer (**Table S4**). Lysates were incubated on ice for 30 minutes, and insoluble material was pelleted at 13,000g for 10 minutes at 4°C. RNA content was quantified using a Nanodrop 2000 spectrophotometer and 100 μg of total RNA per condition was loaded onto a 10-45% sucrose gradient (**Table S4**). Gradients were centrifuged at 40,000 rpm for 1.5 hours at 4°C and were fractionated using a BioComp fractionator (BioComp Instruments, Fredericton NB) into 800 μL fractions that were divided equally for the isolation of either protein or RNA. RNA UV absorbance was quantified across the gradient and peak 43/48S, 60S and 80S absorbance values were calculated for each

experimental replicate by subtracting background absorbance, determined as the lowest absorbance recorded for the *siLinear+5078* gradient in that replicate.

Protein was isolated by overnight ethanol precipitation at -20°C and centrifugation at 20,000g for 25 minutes at 4°C. Pellets were resuspended in RIPA and 1x loading buffer for immunoblotting. RNA was precipitated from each fraction, as well as from the total polysome lysate input, using sodium acetate and ethanol overnight at -80°C. Precipitates were pelleted at 20,000g for 30 minutes at 4°C and RNA was purified by TRIzol/chloroform extraction for subsequent analysis by qPCR or RNA-sequencing.

For the assessment of translational efficiency, equal volumes of RNA from fractions 8-13 (actively translated RNAs) were pooled for sequencing, alongside samples of total input lysate. Samples were polyA enriched and sequenced, with reads processed as described above. Reads corresponding to transcripts annotated for the GRCh38 genome assembly were quantified using featureCounts. Transcripts not expressed in every sample were filtered out, and changes in RNA expression for the remaining transcripts were determined using DESeq2. Transcripts deemed to be translationally regulated were those exhibiting a differential abundance in polysome fractions relative to the si*Control* treatment, despite no significant change in abundance in the corresponding total RNA inputs. Gene set enrichment analysis (GSEA) on selected transcript analysis was performed using Reactome software[25].

Sodium arsenite stress assays

Cells were plated on collagen-coated glass chamber slides or 12 mm coverslips and transfected with siRNAs, as described above. One day after siRNA treatment, cells were treated with either fresh EGM-2 or EGM-2 containing 100 μM of sodium arsenite (Sigma-Aldrich) for 1 hour prior

to fixation and staining, or lysis and immunoblotting for p-eIF2α, as detailed above. For the assessment of stress granules, cells were washed twice with PBS, fixed with 4% paraformaldehyde (PFA, Sigma-Aldrich) for 15 minutes at room temperature, washed twice in PBS with 0.1% Tween (PBST), blocked in 5% BSA in PBST for 1 hour at room temperature, and labeled overnight at 4°C in 1% BSA in PBST containing mouse anti-G3BP1 (BD Biosciences, 1:1000 dilution) and rabbit anti-Caprin-1 (Proteintech, 1:500). The following day, cells were washed twice with PBST and incubated for 1 hour at room temperature in AF568 Donkey anti-mouse and AF647 Donkey anti-rabbit (both ThermoFisher, 1:1000) in 1% BSA in PBST. Nuclei were labeled with 600nM DAPI in PBS for 10 minutes at room temperature and slides were mounted in Mowiol. To quantify stress granule positive cells, a minimum of four independent wide-field epifluorescence images were collected per condition, per replicate. For STED imaging of stress granules, cells were labeled with AF532 Donkey Anti-mouse and AF488 Donkey Anti-rabbit secondary antibodies and slides were mounted in ProLong Diamond Antifade with DAPI.

OPP Assay

Protein synthesis was assessed using the Click-iT Plus OPP protein synthesis kit (ThermoFisher). Briefly, cells were cultured in EGM-2 media, with or without 100 μM of sodium arsenite for 30 minutes prior to incubation with OPP reagent for an additional 30 minutes of culture. Cells were then fixed in 4% PFA and permeabilized with PBST. OPP-containing peptides were labeled with Alexa488, and nuclei labeled with NuclearMask stain as per the manufacturer's instructions. Fluorescence intensity for both stains was determined using a SpectraMax M3 plate reader (Molecular Devices, San Jose, CA). The nuclear signal was used to normalize the OPP derived signal across wells.

Statistical Analysis

All statistical analysis was performed using Graphpad Prism software. Details of the statistical tests used are specified in the figure captions. Data are presented as mean ± SEM. For work in HPAECs, indicated sample sizes are the number of independent experimental replicates. For work in BOECs, indicated sample sizes represent the number of individual human subjects tested.

Results

Profiling the impact of BMPR2 loss on HPAEC circRNA expression with high-depth RNA sequencing

To determine the contribution of circRNAs to the endothelial phenotype of *BMPR2* loss, we first profiled circRNA expression in *BMPR2* silenced and control HPAECs, with and without BMP9 treatment. RNA sequencing was completed at a depth of over 300 million high-quality paired-end reads (600 million individual reads) per sample (**Figure S1**), roughly 10-fold the depth required for standard mRNA differential expression analysis. To profile circRNA expression within this dataset, a junction sequence library was constructed using a publicly available database of 92,369 known or proposed circRNA annotations within the human genome[18], with junction sequences consisting of the 80 bases to the left and right of the unique backsplice site for each circRNA annotation (**Figure 1A**)[21]. Screening reads against this library filtered out over 99.99% of all reads, leaving only those that aligned with circRNA-derived backsplice junctions (**Figures 1B and 1C**). While 19,351 unique circRNA annotations were detected in at least one sample, an additional

filtering of these annotations at a threshold of 0.1 transcripts per kilobase million (TPM) per sample (**Figure 1D**) produced a list of 425 putative circRNAs that are abundantly expressed in HPAECs (**File S1**). These circRNAs represented just over 2% of the annotations, but roughly two thirds of the reads, that were captured from the junction library.

Analysis of these 425 annotations did not yield any differentially expressed targets with BMP9 treatment. However, 27 differentially expressed annotations were identified with *BMPR2* silencing at a *p*-value of less than 0.05, including six annotations with an adjusted *p*-value less than 0.05 (**Figure 1E and Table S6**). RNase R digestion, which preferentially degrades linear transcripts via their 3' termini[26], validated two (*hsa_circ_0005078* and *hsa_circ_0001592*) of these six putative transcripts as true, RNase R resistant circRNAs (**Figure 1F**). Two additional transcripts (*hsa_circ_0013876* and *hsa_circ_0001218*) exhibited partial RNase R resistance relative to the linear RNA control, suggesting the capture of both linear and circular RNA reads for these annotations. Analysis of read alignments for the two annotations that failed RNase R validation (*hsa_circ_0000400* and *hsa_circ_0000320*) identified a bias of these alignments towards segments of their respective junction sequences that were shared with linear mRNA transcripts of the same genomic origin, indicating a misattribution of reads from linear mRNAs (**Figure S2**).

BMPR2 circRNAs regulate endothelial apoptosis and proliferation

Of the two validated circRNA annotations from the differential expression analysis, *hsa_circ_0005078* (*circ5078*) was of particular interest, as it consists of a circularized form of exon 12 from the *BMPR2* locus (**Figure 2A**). A subsequent examination of the 92,369 annotations

assessed in the junction library identified an additional seven *BMPR2*-derived annotations that were detected in at least one sample, of which one, *hsa_circ_0003218* (*circ3218*), was abundantly expressed in HPAECs (**Figure 2B**). Like *circ5078*, *circ3218* was resistant to RNase R digestion (**Figure 2C**). However, while *circ5078* was targeted by the *BMPR2* siRNA pool used in the RNA-sequencing screen (**Figures 2A and 2D**), *circ3218*, which consists of *BMPR2* exons 2 and 3, was unaffected by *BMPR2* siRNA treatment (**Figures 2A and 2E**). An independent validation using lower-depth, publicly available GEO datasets confirmed the existence of *BMPR2b*, *circ5078* and *circ3218* in human, but not mouse endothelium (**Figures S3 and 2F**). Similarly, *circ3218* was the only alternative *BMPR2* transcript to be detected in the rat lung (**Figure 2G**), suggesting that the splicing events responsible for *BMPR2b* and *circ5078* formation do not occur in rodents.

Custom siRNAs targeting specific *BMPR2* transcripts demonstrated efficient depletion of linear *BMPR2* mRNAs (*siLinear*), *circ5078* (*si5078*), or *circ3218* (*si3218*), when compared to the commercially available *BMPR2* siRNA pool (*siLinear+5078*) that targets both linear *BMPR2* transcripts and *circ5078* (**Figures 2A and 2H**). Although both circRNA-specific siRNAs modestly reduced linear *BMPR2* mRNA levels, neither siRNA impacted BMPR-II protein, which was depleted exclusively in the *siLinear* and *siLinear+5078* groups (**Figure 2I**). Silencing of *circ3218*, but not *circ5078*, increased the susceptibility of HPAECs to TNFα and cycloheximide-induced apoptosis (**Figures 2J and S4**). In contrast, *circ5078* depletion significantly enhanced HPAEC proliferation when compared to the non-targeting siRNA control (**Figure 2K**). Interestingly, the combined silencing of *circ5078* and linear *BMPR2* mRNAs eliminated the proliferative effect achieved by silencing *circ5078* alone, suggesting a potential interaction between *circ5078* and linear *BMPR2* mRNA in the regulation of HPAEC proliferation.

The proliferative effect of circ5078 loss is Caprin-1-dependent

An *in silico* BEAM RNA Interaction mOtifs (BRIO)[27] screen for potential *circ5078* protein targets identified three likely binding partners for *circ5078*, including Argonaute 2, Nuclear Cap Binding Subunit 3 (NCBP3) and Caprin-1 (**Figure 3A**). Of these targets, Caprin-1 is a major component of cytoplasmic RNA granules that is known to enhance proliferation via the enhanced translation of cell cycle regulators, including cyclins[28]. RNA-immunoprecipitation for Caprin-1 confirmed its interaction with both *circ5078* and linear *BMPR2* mRNA in HPAECs (**Figure 3B**). Although *circ5078* was not amenable to visualization by custom RNA-FISH probes targeting its unique backsplice junction, this method was successful in validating the co-localization of Caprin-1 and linear *BMPR2* mRNA by super-resolution microscopy (**Figure 3C**).

Depletion of *circ5078* or linear *BMPR2* mRNA had no impact of on the abundance of Caprin-1 protein or its distribution between the cytosol and a membrane-bound fraction containing the endoplasmic reticulum, the two major sites of protein synthesis in the cell (**Figure 3D**). However, *CAPRIN1* silencing did eliminate the excessive proliferation observed in *circ5078*-depleted HPAECs (**Figures 3E and S5**), confirming that this proliferative response is indeed Caprin-1 dependent. Moreover, *circ5078* depletion induced a significant increase in protein levels of the known Caprin-1 translational target, Cyclin-D1 (**Figures 3F and 3G**), despite no elevation in corresponding mRNA levels (**Figure 3H**). As with the proliferative response, the elevation in Cyclin-D1 protein was lost when *circ5078* and linear *BMPR2* mRNA were silenced together, further supporting opposing roles for linear *BMPR2* mRNA and *circ5078* in the regulation of endothelial proliferation and translational control.

circ5078 and linear BMPR2 RNA influence ribosome assembly and translational initiation

The impact of *circ5078* and linear *BMPR2* RNA depletion on endothelial translation was assessed by sucrose-gradient ultracentrifugation, which quantified free ribosomal subunits (Fractions 2-4), 80S monosomes (Fraction 5), and actively translating polysomes (Fractions 6-13) in control and silenced HPAECs (**Figure 4A**), as well as the co-sedimentation of proteins (**Figure 4B**) and RNAs associated with these complexes. Examination of RNA UV absorbance identified a baseline impairment of ribosomal assembly in control HPAECs, defined by the presence of polysome half-mers and an accumulation of 43/48S preinitiation complexes (PIC) that are marked by the initiation factor subunit, eIF3B, in Fraction 3 (**Figures 4B-4D**). This impaired assembly was not linked to a deficiency of 60S ribosomal subunits[29] in control HPAECs, but was associated with an accumulation of Caprin-1, which co-sedimented with *circ5078* in Fractions 2 and 3 of the control gradients (**Figures 4B-4E**). Silencing linear *BMPR2* mRNA or *circ5078* reduced the abundance of Caprin-1 in these fractions and enhanced ribosomal assembly, with the greatest effect observed with the combined silencing of both linear and circular *BMPR2* transcripts.

While this effect on ribosome assembly suggests that depletion of both *circ5078* and linear *BMPR2* mRNA can enhance translation, HPAECs lacking linear *BMPR2* mRNA, either alone or in combination with *circ5078* silencing, also exhibited an accumulation of 80S monosomes (**Figures 4A and 4D**) that is indicative of a separate block on translational initiation in this condition. Examination of the initiation factor, eIF2α, which shuttles Met-$tRNA_i^{Met}$ to the PIC, showed no impact of linear *BMPR2* mRNA depletion on the abundance of PIC-associated eIF2α in Fraction 3, but did identify a loss of free eIF2α in Fraction 2, both with linear *BMPR2* mRNA depletion alone and in the pooled silencing condition (**Figure 4B**). These findings point to a

potential defect in eIF2α turnover as a limitation on translational initiation that counterbalances enhanced ribosome assembly when linear *BMPR2* mRNA is lost.

Profiling of Cyclin-D1 mRNA within the sucrose gradients also supported a shift in translational efficiency under the various silencing conditions, from a predominance of monosome associated transcripts in control HPAECs, towards an accumulation in more highly translated polysome fractions under conditions where *circ5078* was silenced (**Figure 4F**). Interestingly, this shift was not reversed with pooled siRNA treatment, despite baseline Cyclin-D1 protein levels in this condition. Moreover, quantification of O-propargyl-puromycin (OPP) incorporation in control and silenced HPAECs identified no impact of *circ5078* or linear *BMPR2* RNA depletion on total protein synthesis, both at baseline or in response to sodium arsenite-induced oxidative stress (**Figures 4A and S6**), suggesting that any effects on translational efficiency do not impact the entire proteome, and are instead limited to a specific subset of endothelial transcripts.

circ5078 is a broad regulator of endothelial translational efficiency

To identify the specific transcripts that are translationally regulated by *circ5078* or linear *BMPR2* mRNA depletion, we sequenced polyadenylated RNA from actively translated polysome fractions (Fractions 8-13) for each siRNA condition. Total polyadenylated RNA from input lysates was also sequenced to control for changes in overall transcript abundance arising from siRNA treatment (**Figure 5A**). For each siRNA condition, differential expression analysis was performed on both the polysome and total input samples relative to their respective non-targeting siRNA controls (**Figure S7**) and differentially translated genes were identified as those not altered in the input samples ($p_{adj} \geq 0.05$), but exhibiting differential abundance in the polysome fraction ($p_{adj} < 0.05$)

(**Figure 5B and File S2**). This analysis identified 1,137 differentially translated mRNAs across all treatment groups. Of these transcripts, few were shared between the individual siRNA treatments, and more than half were unique to *circ5078* silencing (**Figures 5C and 5D**).

Although the 665 transcripts impacted by *circ5078* were split evenly between those that were enriched in polysomes, and those that were under-represented in these fractions (**Figure 5D**), gene set enrichment analysis (GSEA) using Reactome[25] found no enrichment of pathways that were translationally repressed by *circ5078* depletion. In contrast, this analysis did identify an upregulation of pathways regulating mitochondrial translational processes (**Figure 5E**), driven by the enrichment of 10 nuclear genes encoding mitochondrial ribosome subunits. A subsequent comparison of transcript abundance in the polysome fraction across all four siRNA conditions confirmed that 7 of these 10 targets were uniquely upregulated with *circ5078* depletion (**Figure 5F**), providing a potential mechanism by which *circ5078* can regulate endothelial proliferation through changes in cellular energetics.

BMPR2 transcripts differentially regulate Caprin-1 stress granule formation

Despite our identification of altered eIF2α sedimentation with linear *BMPR2* mRNA depletion, as well as previous reports of reduced stress-induced eIF2α phosphorylation with *BMPR2* loss[5], silencing of linear *BMPR2* mRNA or *circ5078* did not impact eIF2α phosphorylation at baseline, or alter the degree of phosphorylation in response to arsenite-induced stress (**Figures 6A and 6B**). However, silencing linear *BMPR2* mRNA did reproduce published reports of reduced stress granule formation in *BMPR2*-deficient HPAECs, as determined by Caprin-1 and G3BP-1 co-localization (**Figures 6C and 6D**). In keeping with its effects on proliferation and translation,

circ5078 depletion had the opposite effect, enhancing the percentage of stress granule-positive cells by nearly three-fold. Pooled silencing of both transcripts returned stress granules to control levels, despite the complete absence of BMPR-II protein in these cells. These findings were supported by STED super-resolution microscopy for Caprin-1 and G3BP-1, which confirmed the reduced size, density, and abundance of stress granules in granule-positive HPAECs lacking linear *BMPR2* mRNA, the opposite effect in *circ5078*-silenced cells, and a return to control levels in HPAECs lacking both transcripts (**Figures 6E and S8**).

In order to confirm the relevance of these studies to the endothelial phenotype of PAH, blood outgrowth endothelial cells (BOECs) from *BMPR2* mutation-bearing PAH patients were assessed for *BMPR2* transcript expression, and were found to be deficient in linear *BMPR2* transcripts, but not *circ5078* (**Figure 6F**). This shift in the balance between linear *BMPR2* and *circ5078* was accompanied by reduced stress granule formation in arsenite-treated cells from PAH patients, mirroring the effect seen by silencing linear *BMPR2* mRNA in HPAECs (**Figures 6G and S9A**). More critically, rebalancing circular and linear transcripts through *circ5078* depletion rescued this phenotype to control levels (**Figures 6H and S9B**), confirming that the diseased stress response in these cells is more dependent on the relative abundance of *BMPR2* transcripts than the loss of the protein receptor.

Discussion

There is abundant evidence linking genetic drivers of pulmonary vascular disease to altered translational control. In addition to previous reports of impaired stress-induced eIF2α phosphorylation, prolonged p38 MAPK signaling, and increased GADD34–PP1 activity with *BMPR2* loss[5], biallelic mutations in *EIF2AK4*, the gene encoding the eIF2α kinase, GCN2, have also been identified in patients with pulmonary veno-occlusive disease (PVOD), alongside compound heterozygous *EIF2AK4*/*BMPR2* mutations in a small group of PAH patients[30]. Moreover, reduced GCN2 expression is observed in both PVOD and PAH patients, with or without mutations in *EIF2AK4* or *BMPR2*[31]. By identifying *circ5078* as a novel *BMPR2*-derived functional RNA and defining its role as a regulator of endothelial proliferation, translation and stress responses, our work demonstrates a more nuanced role for *BMPR2* loss in endothelial dysfunction that arises through the integrated and opposing actions of linear and circular *BMPR2* transcripts. Importantly, these findings offer the prospect that certain elements of the endothelial PAH phenotype, which were previously attributed to a loss of the BMPR-II protein receptor, are instead driven by an imbalance in the functional effects of these RNAs.

Our work profiling polysome gradients identified two seemingly discreet impacts of *BMPR2* transcript silencing on endothelial translation; a Caprin-1 associated enhancement of ribosome assembly with depletion of either linear *BMPR2* mRNA or *circ5078*, and a translational block linked to 80S monosome accumulation and altered eIF2α turnover that was exclusively dependent on linear *BMPR2* loss. The integration of these effects, one enhancing translation, and the other repressing it, provides a model to explain the observed effects on proliferation, translation and stress responses under our different silencing conditions. Importantly, these changes were not

accompanied by a difference in overall protein synthesis or eIF2α phosphorylation, either under baseline conditions or in response to arsenite-induced stress.

It is important to note that the absence of differential eIF2α phosphorylation in our studies may be dependent on the nature of the cellular stress employed, as previous studies examining eIF2α phosphorylation with *BMPR2* loss focused primarily on TNFα-induced stress responses[5]. Although GCN2 can be activated in response to the oxidative stress arising from sodium arsenite, its activity is more commonly associated with amino acid depravation[32]. Beyond phosphorylation of the eIF2α subunit, our findings may also point to a potential role for other known regulators of eIF2 turnover, including the altered activity of the eIF2 guanine nucleotide exchange factor, eIF2B, which is essential for eIF2 recycling into new ternary complexes[33], or the eIF2 GTPase-activating protein and guanine nucleotide dissociation inhibitor, eIF5, which catalyses the release of initiation factors upon ribosome assembly[34]. Further studies exploring the activity of these factors with linear *BMPR2* mRNA depletion are merited.

The identification of 80S monosome accumulation is also not exclusively linked to translational inactivity. Recent reports have instead demonstrated that transcripts bound by a single ribosome are often biased towards the translation of short open reading frames, nonsense-mediated decay targets, low abundance regulatory proteins, and upstream open reading frames that serve as a fundamental component of the translational stress response[35]. Monosome accumulation can also arise from ribosomal stalling or other initiation defects that are not easily assessed using the analysis of polysome profiles in sucrose gradients. The application of more sophisticated approaches, such as ribosome footprinting, would aid in determining not only the transcripts accumulating in this 80S peak, but the precise location of the ribosomes on these transcripts.

The identification of Caprin-1 as an interacting partner with both *circ5078* and linear *BMPR2* mRNA is of particular interest, as this protein has been identified in cancer for its role in the enhanced translation of cell cycle regulators[36]. In addition to the potential effect of *BMPR2* transcript depletion on the translation of Cyclin-D1, we also identified a number of mitoribosomal genes that are enhanced exclusively with *circ5078* depletion. Imbalance in mitochondrial-versus nuclear-encoded mitochondrial proteins, known as the mitonuclear imbalance, has been reported in both disease and ageing[37], providing potential mechanistic link between the excessive translation of these genes, altered endothelial metabolic function, and excessive proliferation. It was also noteworthy that silencing of linear *BMPR2* mRNA or *circ5078*, either alone or together, dramatically altered both the sedimentation of Caprin-1 with ribosomal initiation complexes and its incorporation into stress granules, despite no impact on eIF2α phosphorylation. Although stress granules and eIF2α phosphorylation are often observed in concert under stressed conditions, this finding agrees with previous studies showing that Caprin-1 deletion or overexpression can directly modulate stress granule frequency, independent of any effects on eIF2α phosphorylation and translational initiation[28].

In addition to the identification and functional characterization of *circ5078*, this work also provides the first known profile of circRNA expression in the human pulmonary endothelium. This profile can serve as a useful tool for understanding the contribution of circRNAs to endothelial cell function in health and disease. The approach of screening high-depth RNA sequencing data for backsplice junction-spanning reads offers several advantages over alternatives like RNase R pre-treatment or commercially available circRNA microarrays[38,39]. While the infrequency of junction-spanning reads within these datasets requires extremely high read depths to achieve the statistical power needed for differential expression analysis, the absence of

enzymatic digestion steps minimizes sample degradation and facilitates a more accurate quantification of circular transcripts. This approach also allows for the parallel quantification of circRNAs alongside traditional linear RNA, and is not limited to quantifying a predetermined set of circRNAs, as is the case with circRNA microarrays. Instead, datasets can be mined for previously unexplored circRNA annotations, or retroactively analyzed to assess newly characterized circRNA annotations that were not included in the original analysis.

Limitations of the study

While our study provides important new insights into the contribution of both *circ5078* and linear *BMPR2* mRNA to endothelial translation, it also raises many new questions that each require a detailed follow-up investigation. We have validated the interaction of Caprin-1 with both linear and circular *BMPR2* RNA by RNA-immunoprecipitation, and have shown that the proliferative phenotype arising from *circ5078* depletion is indeed Caprin-1 dependent. However, additional studies, such as PAR-CLIP analysis, are needed to confirm a direct interaction of Caprin-1 with *BMPR2* transcripts in HPAECs, and define the precise mechanism by which these interactions regulate ribosome assembly. Moreover, as the silencing of linear *BMPR2* mRNA results in a loss of both the transcript and its resultant protein, it is unclear to what degree each of these macromolecules contributes to the endothelial phenotype of *BMPR2* loss. Our demonstration of restored stress granule formation in PAH patient BOECs with *circ5078* depletion, despite no change in BMPR-II levels, indicates that loss of the protein receptor may be necessary, but is not sufficient for this component of the endothelial stress response. Additional rescue studies involving the restoration of patient cells with linear *BMPR2* mRNA variants encoding wildtype, kinase dead, or exon 12-deficient forms of BMPR-II would address this question by dissecting the relative contributions of the RNA, versus its protein product, to the disease-linked cellular phenotype.

Data Availability

Data supporting this work is available upon request from the corresponding author, MLO. Sequencing data will be made publicly available upon the publication of this manuscript.

Funding

This work was supported by funding from the Canadian Institutes of Health Research (CIHR; PJT-178078). MMV would like to acknowledge graduate scholarship support from CIHR and the Canadian Vascular Network.

Acknowledgements

The authors would like to acknowledge Ariana Bacelar-Jimenez, Dr. Lindsey Hawke and Dr. Kathrin Tyryshkin for their technical support, as well as Dr. Lynne Postovit for assistance with the sucrose gradient fractionation studies.

Refergences

1. Cober, N.D., VandenBroek, M.M., Ormiston, M.L., and Stewart, D.J. (2022). Evolving Concepts in Endothelial Pathobiology of Pulmonary Arterial Hypertension. Hypertension *79*, 1580-1590. 10.1161/HYPERTENSIONAHA.122.18261.

2. Lavoie, J.R., Ormiston, M.L., Perez-Iratxeta, C., Courtman, D.W., Jiang, B., Ferrer, E., Caruso, P., Southwood, M., Foster, W.S., Morrell, N.W., and Stewart, D.J. (2014). Proteomic analysis implicates translationally controlled tumor protein as a novel mediator of occlusive vascular remodeling in pulmonary arterial hypertension. Circulation *129*, 2125-2135. 10.1161/CIRCULATIONAHA.114.008777.

3. Toshner, M., Voswinckel, R., Southwood, M., Al-Lamki, R., Howard, L.S., Marchesan, D., Yang, J., Suntharalingam, J., Soon, E., Exley, A., et al. (2009). Evidence of dysfunction of endothelial progenitors in pulmonary arterial hypertension. Am J Respir Crit Care Med *180*, 780-787. 200810-1662OC [pii] 10.1164/rccm.200810-1662OC.

4. Long, L., Ormiston, M.L., Yang, X., Southwood, M., Graf, S., Machado, R.D., Mueller, M., Kinzel, B., Yung, L.M., Wilkinson, J.M., et al. (2015). Selective enhancement of endothelial BMPR-II with BMP9 reverses pulmonary arterial hypertension. Nat Med *21*, 777-785. 10.1038/nm.3877.

5. Sawada, H., Saito, T., Nickel, N.P., Alastalo, T.P., Glotzbach, J.P., Chan, R., Haghighat, L., Fuchs, G., Januszyk, M., Cao, A., et al. (2014). Reduced BMPR2 expression induces GM-CSF translation and macrophage recruitment in humans and mice to exacerbate pulmonary hypertension. J Exp Med *211*, 263-280. 10.1084/jem.20111741.

6. Machado, R.D., Aldred, M.A., James, V., Harrison, R.E., Patel, B., Schwalbe, E.C., Gruenig, E., Janssen, B., Koehler, R., Seeger, W., et al. (2006). Mutations of the TGF-beta type II receptor BMPR2 in pulmonary arterial hypertension. Hum Mutat *27*, 121-132. 10.1002/humu.20285.

7. Graf, S., Haimel, M., Bleda, M., Hadinnapola, C., Southgate, L., Li, W., Hodgson, J., Liu, B., Salmon, R.M., Southwood, M., et al. (2018). Identification of rare sequence variation underlying heritable pulmonary arterial hypertension. Nat Commun *9*, 1416. 10.1038/s41467-018-03672-4.

8. Machado, R.D., Southgate, L., Eichstaedt, C.A., Aldred, M.A., Austin, E.D., Best, D.H., Chung, W.K., Benjamin, N., Elliott, C.G., Eyries, M., et al. (2015). Pulmonary Arterial Hypertension: A Current Perspective on Established and Emerging Molecular Genetic Defects. Hum Mutat *36*, 1113-1127. 10.1002/humu.22904.

9. Humbert, M., Sitbon, O., Chaouat, A., Bertocchi, M., Habib, G., Gressin, V., Yaici, A., Weitzenblum, E., Cordier, J.F., Chabot, F., et al. (2006). Pulmonary arterial hypertension in France: results from a national registry. Am J Respir Crit Care Med *173*, 1023-1030. 10.1164/rccm.200510-1668OC.

10. Badesch, D.B., Raskob, G.E., Elliott, C.G., Krichman, A.M., Farber, H.W., Frost, A.E., Barst, R.J., Benza, R.L., Liou, T.G., Turner, M., et al. (2010). Pulmonary arterial hypertension: baseline characteristics from the REVEAL Registry. Chest *137*, 376-387. 10.1378/chest.09-1140.

11. Larkin, E.K., Newman, J.H., Austin, E.D., Hemnes, A.R., Wheeler, L., Robbins, I.M., West, J.D., Phillips, J.A., 3rd, Hamid, R., and Loyd, J.E. (2012). Longitudinal analysis casts doubt on the presence of genetic anticipation in heritable pulmonary arterial hypertension. Am J Respir Crit Care Med *186*, 892-896. 10.1164/rccm.201205-0886OC.

12. Theilmann, A.L., Hawke, L.G., Hilton, L.R., Whitford, M.K.M., Cole, D.V., Mackeil, J.L., Dunham-Snary, K.J., Mewburn, J., James, P.D., Maurice, D.H., et al. (2020). Endothelial BMPR2 Loss Drives a Proliferative Response to BMP (Bone Morphogenetic Protein) 9 via Prolonged Canonical Signaling. Arterioscler Thromb Vasc Biol *40*, 2605-2618. 10.1161/ATVBAHA.119.313357.

13. de Jesus Perez, V., Yuan, K., Alastalo, T.P., Spiekerkoetter, E., and Rabinovitch, M. (2014). Targeting the Wnt signaling pathways in pulmonary arterial hypertension. Drug Discov Today *19*, 1270-1276. 10.1016/j.drudis.2014.06.014.

14. Ormiston, M.L., Upton, P.D., Li, W., and Morrell, N.W. (2015). The promise of recombinant BMP ligands and other approaches targeting BMPR-II in the treatment of pulmonary arterial hypertension. Glob Cardiol Sci Pract *2015*, 47. 10.5339/gcsp.2015.47.

15. Wieser, R., Attisano, L., Wrana, J.L., and Massague, J. (1993). Signaling activity of transforming growth factor beta type II receptors lacking specific domains in the cytoplasmic region. Mol Cell Biol *13*, 7239-7247. 10.1128/mcb.13.12.7239-7247.1993.

16. Nishihara, A., Watabe, T., Imamura, T., and Miyazono, K. (2002). Functional heterogeneity of bone morphogenetic protein receptor-II mutants found in patients with primary pulmonary hypertension. Mol Biol Cell *13*, 3055-3063. 10.1091/mbc.e02-02-0063.

17. Patop, I.L., Wust, S., and Kadener, S. (2019). Past, present, and future of circRNAs. EMBO J *38*, e100836. 10.15252/embj.2018100836.

18. Glazar, P., Papavasileiou, P., and Rajewsky, N. (2014). circBase: a database for circular RNAs. RNA *20*, 1666-1670. 10.1261/rna.043687.113.

19. Pandey, P.R., Munk, R., Kundu, G., De, S., Abdelmohsen, K., and Gorospe, M. (2020). Methods for analysis of circular RNAs. Wiley Interdiscip Rev RNA *11*, e1566. 10.1002/wrna.1566.

20. Bolger, A.M., Lohse, M., and Usadel, B. (2014). Trimmomatic: a flexible trimmer for Illumina sequence data. Bioinformatics *30*, 2114-2120. 10.1093/bioinformatics/btu170.

21. Cooper, D.A., Cortes-Lopez, M., and Miura, P. (2018). Genome-Wide circRNA Profiling from RNA-seq Data. Methods Mol Biol *1724*, 27-41. 10.1007/978-1-4939-7562-4_3.

22. Langmead, B., and Salzberg, S.L. (2012). Fast gapped-read alignment with Bowtie 2. Nat Methods *9*, 357-359. 10.1038/nmeth.1923.

23. Liao, Y., Smyth, G.K., and Shi, W. (2014). featureCounts: an efficient general purpose program for assigning sequence reads to genomic features. Bioinformatics *30*, 923-930. 10.1093/bioinformatics/btt656.

24. Love, M.I., Huber, W., and Anders, S. (2014). Moderated estimation of fold change and dispersion for RNA-seq data with DESeq2. Genome Biol *15*, 550. 10.1186/s13059-014-0550-8.

25. Gillespie, M., Jassal, B., Stephan, R., Milacic, M., Rothfels, K., Senff-Ribeiro, A., Griss, J., Sevilla, C., Matthews, L., Gong, C., et al. (2022). The reactome pathway knowledgebase 2022. Nucleic Acids Res *50*, D687-D692. 10.1093/nar/gkab1028.

26. Suzuki, H., Zuo, Y., Wang, J., Zhang, M.Q., Malhotra, A., and Mayeda, A. (2006). Characterization of RNase R-digested cellular RNA source that consists of lariat and circular RNAs from pre-mRNA splicing. Nucleic Acids Res *34*, e63. 10.1093/nar/gkl151.

27. Guarracino, A., Pepe, G., Ballesio, F., Adinolfi, M., Pietrosanto, M., Sangiovanni, E., Vitale, I., Ausiello, G., and Helmer-Citterich, M. (2021). BRIO: a web server for RNA sequence and structure motif scan. Nucleic Acids Res *49*, W67-W71. 10.1093/nar/gkab400.

28. Solomon, S., Xu, Y., Wang, B., David, M.D., Schubert, P., Kennedy, D., and Schrader, J.W. (2007). Distinct structural features of caprin-1 mediate its interaction with G3BP-1 and its induction of phosphorylation of eukaryotic translation initiation factor 2alpha, entry to cytoplasmic stress granules, and selective interaction with a subset of mRNAs. Mol Cell Biol *27*, 2324-2342. 10.1128/MCB.02300-06.

29. Rotenberg, M.O., Moritz, M., and Woolford, J.L., Jr. (1988). Depletion of Saccharomyces cerevisiae ribosomal protein L16 causes a decrease in 60S ribosomal subunits and formation of half-mer polyribosomes. Genes Dev *2*, 160-172. 10.1101/gad.2.2.160.

30. Hadinnapola, C., Bleda, M., Haimel, M., Screaton, N., Swift, A., Dorfmuller, P., Preston, S.D., Southwood, M., Hernandez-Sanchez, J., Martin, J., et al. (2017). Phenotypic Characterization of EIF2AK4 Mutation Carriers in a Large Cohort of Patients Diagnosed Clinically With Pulmonary Arterial Hypertension. Circulation *136*, 2022-2033. 10.1161/CIRCULATIONAHA.117.028351.

31. Nossent, E.J., Antigny, F., Montani, D., Bogaard, H.J., Ghigna, M.R., Lambert, M., Thomas de Montpreville, V., Girerd, B., Jais, X., Savale, L., et al. (2018). Pulmonary vascular remodeling patterns and expression of general control nonderepressible 2 (GCN2) in pulmonary veno-occlusive disease. J Heart Lung Transplant *37*, 647-655. 10.1016/j.healun.2017.09.022.

32. Anda, S., Zach, R., and Grallert, B. (2017). Activation of Gcn2 in response to different stresses. PloS one *12*, e0182143. 10.1371/journal.pone.0182143.

33. Pavitt, G.D., Ramaiah, K.V., Kimball, S.R., and Hinnebusch, A.G. (1998). eIF2 independently binds two distinct eIF2B subcomplexes that catalyze and regulate guanine-nucleotide exchange. Genes Dev *12*, 514-526. 10.1101/gad.12.4.514.

34. Paulin, F.E., Campbell, L.E., O'Brien, K., Loughlin, J., and Proud, C.G. (2001). Eukaryotic translation initiation factor 5 (eIF5) acts as a classical GTPase-activator protein. Curr Biol *11*, 55-59. 10.1016/s0960-9822(00)00025-7.

35. Heyer, E.E., and Moore, M.J. (2016). Redefining the Translational Status of 80S Monosomes. Cell *164*, 757-769. 10.1016/j.cell.2016.01.003.

36. Yang, Z.S., Qing, H., Gui, H., Luo, J., Dai, L.J., and Wang, B. (2019). Role of caprin-1 in carcinogenesis. Oncol Lett *18*, 15-21. 10.3892/ol.2019.10295.

37. Houtkooper, R.H., Mouchiroud, L., Ryu, D., Moullan, N., Katsyuba, E., Knott, G., Williams, R.W., and Auwerx, J. (2013). Mitonuclear protein imbalance as a conserved longevity mechanism. Nature *497*, 451-457. 10.1038/nature12188.

38. Zhang, Z.H., Jhaveri, D.J., Marshall, V.M., Bauer, D.C., Edson, J., Narayanan, R.K., Robinson, G.J., Lundberg, A.E., Bartlett, P.F., Wray, N.R., and Zhao, Q.Y. (2014). A comparative study of techniques for differential expression analysis on RNA-Seq data. PLoS One *9*, e103207. 10.1371/journal.pone.0103207.

39. Liu, Y., Zhou, J., and White, K.P. (2014). RNA-seq differential expression studies: more sequence or more replication? Bioinformatics *30*, 301-304. 10.1093/bioinformatics/btt688.

Figures

Figure 1

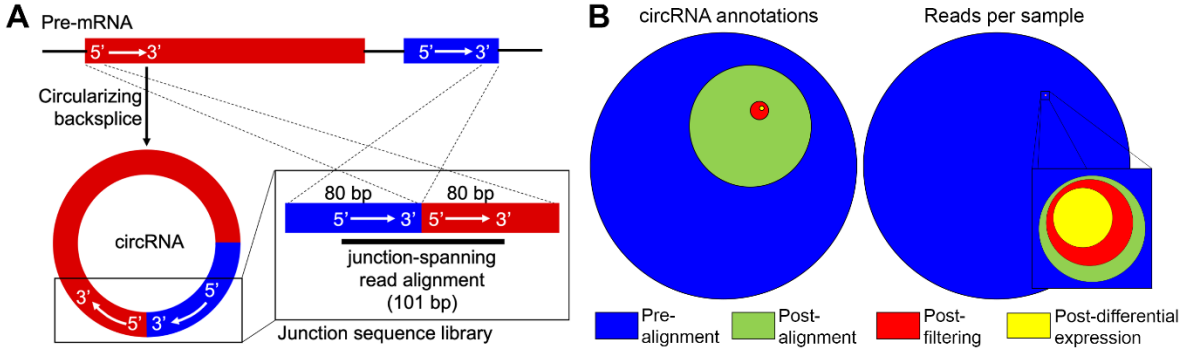

C

Stage	circRNA annotations	Average reads per sample
Pre-Alignment	92,369	624,520,082
Post-Alignment	19,351	44,755
Post-Filtering	425	29,523
Post-Differential Expression	27 ($p < 0.05$) 6 ($p_{adj} < 0.05$)	13,968 ($p < 0.05$) 7,666 ($p_{adj} < 0.05$)

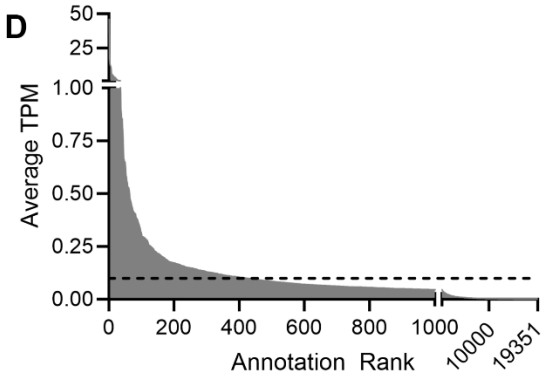

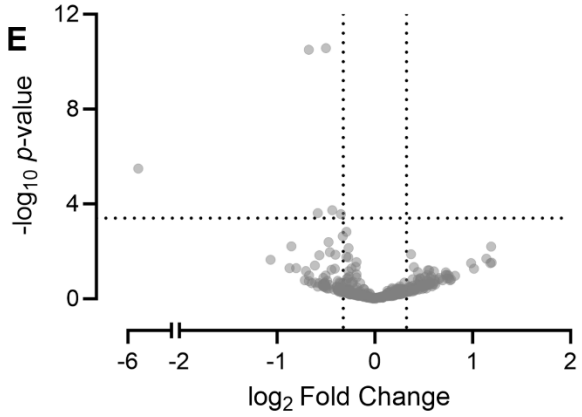

circRNA Annotation	Nearby Gene	Log_2 Fold Change	p_{adj}
hsa_circ_0000400	*TUBA1B*	-0.5006	6.72×10^{-9}
hsa_circ_0000320	*AHNAK*	-0.6771	6.72×10^{-9}
hsa_circ_0005078	*BMPR2*	-5.0455	4.59×10^{-4}
hsa_circ_0013876	*NBPF10*	-0.4362	0.0192
hsa_circ_0001218	*AP1B1*	-0.5833	0.0192
hsa_circ_0001592	*H2AC11*	-0.3465	0.0192

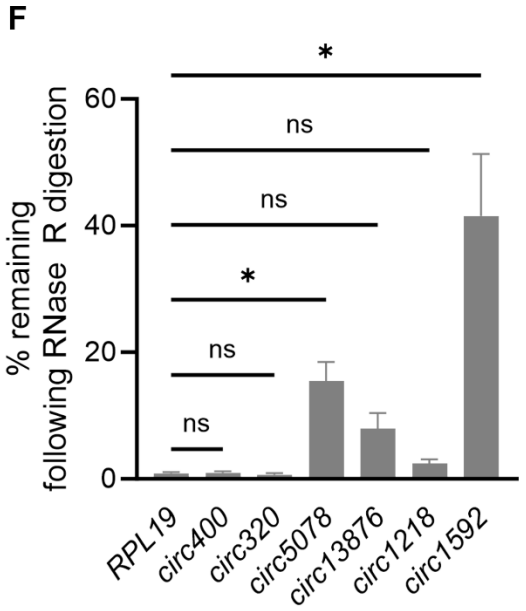

Figure 1. Screening of an ultra-deep RNA-sequencing dataset to profile HPAEC circRNA expression. (A) Schematic of bioinformatic analysis method used to identify circRNA-derived sequencing reads. **(B)** Graphical representation and **(C)** summary of the number of circRNA

annotations and reads per sample at each stage of analysis. **(D)** circRNA annotations ranked by average transcripts per kilobase million (TPM) across 12 samples. An average TPM ≥ 0.1 was selected as the cut-off of abundantly expressed circRNA annotations, as indicated by the dashed line. **(E)** Volcano plot demonstrating the impact of *BMPR2* silencing on the expression of 425 abundantly expressed circRNAs (red circles in **B**). Annotations with $p_{adj} < 0.05$ are summarised. **(F)** RNase R validation of differentially-expressed circRNA annotations alongside *RPL19* as linear RNA control (n=7). **(F)** One-way ANOVA with Dunnett's post-hoc test. ns indicates not significant. $*p \leq 0.05$.

Figure 2

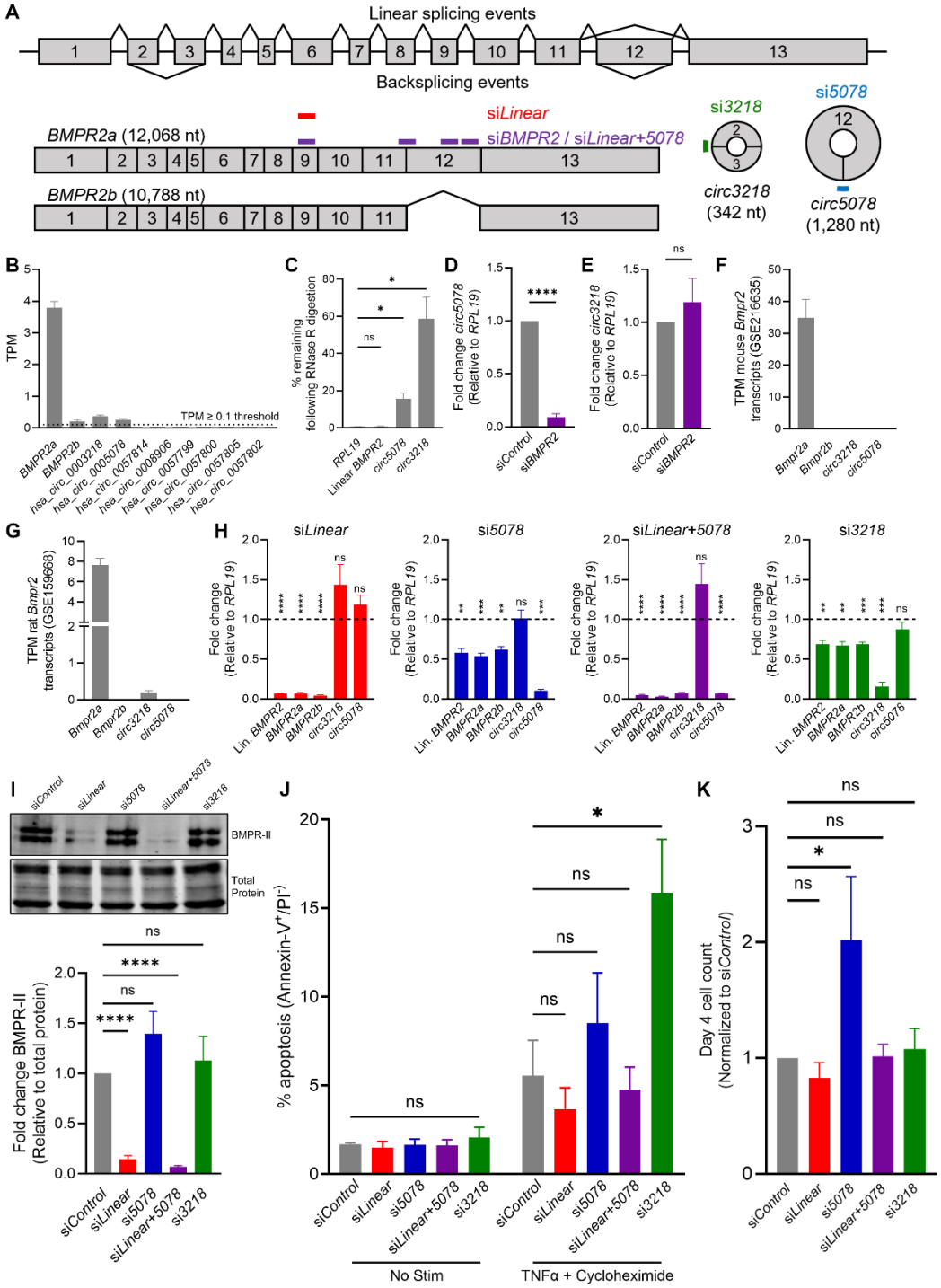

Figure 2. Identification and functional characterization of *BMPR2* derived circRNAs. (A) Summary of all linear and circular *BMPR2*-derived transcripts expressed in HPAECs. Regions targeted by siRNAs used in this study are indicated. **(B)** Relative expression of linear *BMPR2* transcripts and the 8 circRNA annotations that were detected from the RNA-seq screen (n=12). Dashed line indicates expression cutoff of 0.1 transcripts per kilobase million (TPM). **(C)** RNase

R validation of *BMPR2*-derived circRNA annotations, alongside linear *BMPR2* mRNA and *RPL19* as a linear RNA control (n=6). **(D)** Relative expression of *circ5078* and **(E)** *circ3218* in HPAECs treated with pooled siRNAs targeting *BMPR2* (si*BMPR2*) or a non-targeting siRNA control pool (si*Control*) (n=5). **(F)** Quantification of human *BMPR2* transcript equivalents in RNA-sequencing data from mouse endothelial cells (GSE216635, n=4) and **(G)** rat lungs (GSE159668, n=6). **(H)** Impact of si*Linear* (n=4), si*5078* (n=6) si*Linear+5078* (n=5) and si*3218* (n=6) on the abundance of generic linear *BMPR2*, and individual *BMPR2* transcripts. Dashed line represents the expression of each transcript in the si*Control* sample, bars represent the expression of each transcript under the respective knockdown condition. **(I)** Representative immunoblot and quantification of BMPR-II protein expression under each knockdown condition (n=7). **(J)** Percentage of Annexin-V^+/PI^- apoptotic cells under each siRNA condition, with and without a TNFα and cycloheximide apoptotic stimulus (n=7). **(K)** Relative change in cell number over 96 hours for each siRNA treatment relative to si*Control*. **(C, I)** One-way ANOVA with Dunnett's post hoc test. **(D, E)** Paired t-test. **(H)** Two-way ANOVA with Bonferroni post hoc test. **(J)** Two-way ANOVA with Dunnett's post hoc test. **(K)** Mixed effects model with Dunnett's post hoc test. ns indicates not significant. *$p \leq 0.05$, **$p < 0.01$, ***$p < 0.001$, ****$p < 0.0001$.

Figure 3

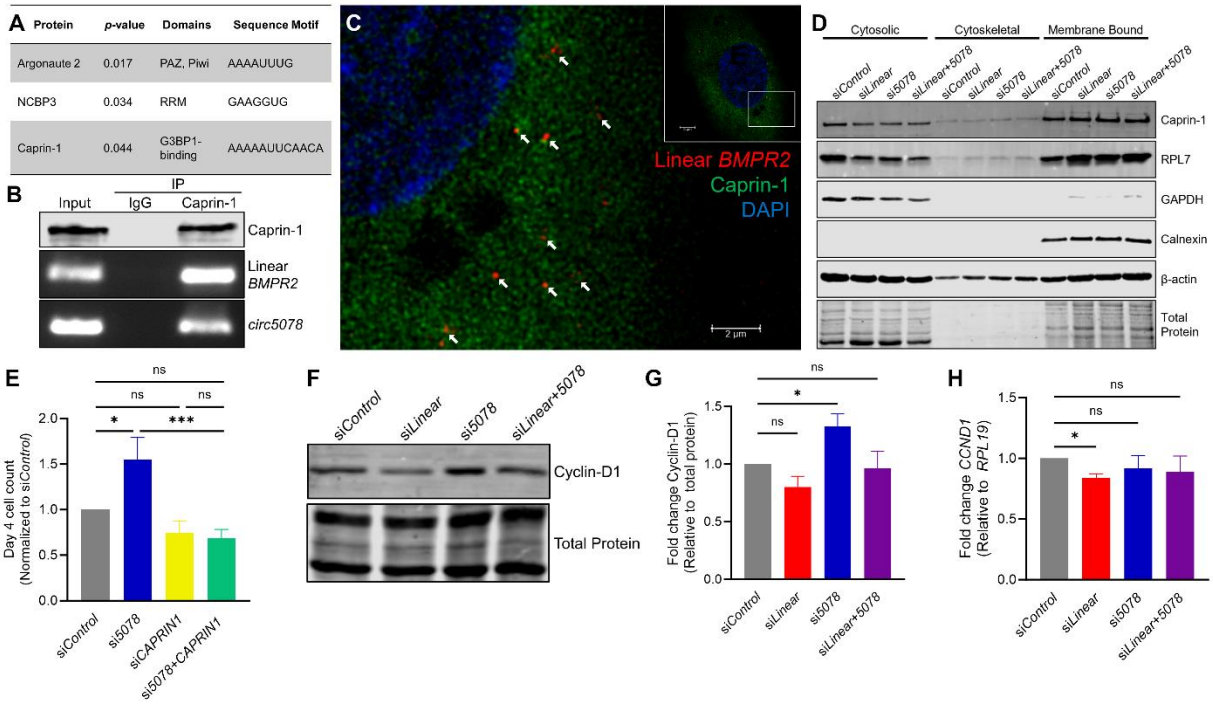

Figure 3. Regulation of proliferation by *circ5078* is Caprin-1 dependent. (A) Potential *circ5078* protein binding partners identified by BRIO. **(B)** RNA-immunoprecipitation of linear *BMPR2* mRNA and *circ5078* with anti-Caprin-1 antibody or IgG control. **(C)** Stimulated emission depletion (STED) microscopy of HPAECs, with Caprin-1 protein labeled by immunocytochemistry (green) and linear *BMPR2* RNA labeled by fluorescent *in situ* hybridization (red). **(D)** Representative immunoblot demonstrating Caprin-1 protein abundance following treatment with siRNAs targeting linear *BMPR2* mRNA (si*Linear*), *circ5078* (si*5078*), a pool targeting all *BMPR2* transcripts (si*Linear+5078*), or a non-targeting control (si*Control*). **(E)** 96-hour cell count for HPAECs following silencing of *circ5078*, *CAPRIN1*, or both transcripts, relative to si*Control* (n=8). **(F)** Representative immunoblot and **(G)** quantification of Cyclin-D1 protein following treatment with si*Control* (grey), *siLinear* (red), *si5078* (blue), or *siLinear+5078* (purple) siRNAs (n=11). **(H)** *CCND1* gene expression under each siRNA condition (n=5). **(E)** One-way ANOVA with Bonferroni post hoc test. **(G, H)** One-way ANOVA with Dunnett's post hoc test. ns indicates not significant. *$p \leq 0.05$, ***$p < 0.001$.

Figure 4

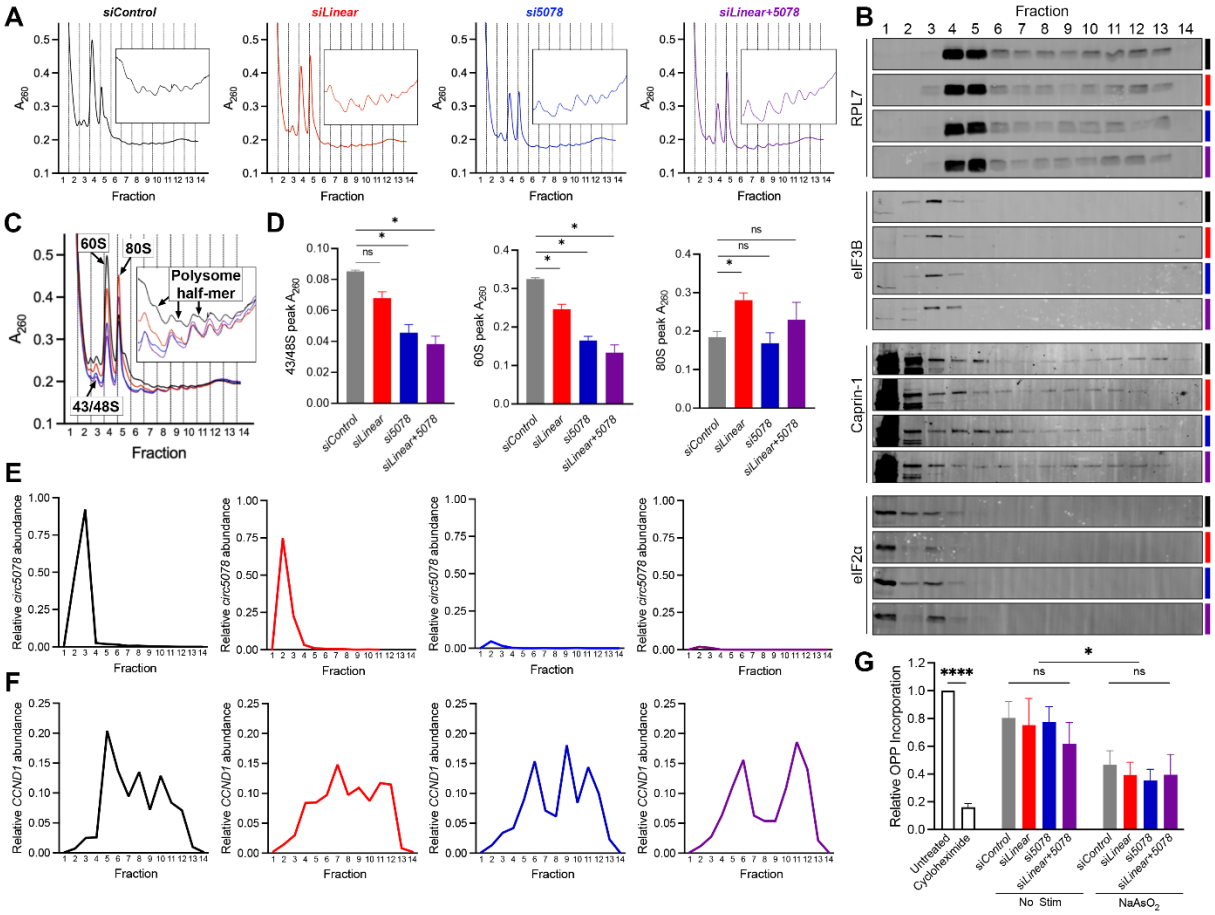

Figure 4. *BMPR2* transcripts regulate ribosomal assembly, composition, and initiation. (A) Sucrose gradient UV absorbance (A_{260}) profiles for HPAECs treated with si*Control* (black), *siLinear* (red), *si5078* (blue), or *siLinear+5078* (purple) siRNAs. Profiles represent the pooled average of 3 independent experiments. Insets are magnification of the curves in fractions 6-12. **(B)** Representative immunoblots from n=3 experiments quantifying RPL7, eIF3B, Caprin-1 and eIF2α abundance across gradient fractions. **(C)** Overlaid A_{260} profiles highlighting the 43/48S preinitiation complex (PIC), 60S ribosomal subunits, 80S monosomes and polysome half-mers, **(D)** Quantification of absorbance less background for the peaks detailed in **C**. One-way ANOVA with Dunnett's post hoc test (n=3). **(E)** Relative abundance of *circ*5078 and **(F)** *CCND1* RNA across all fractions in each siRNA condition. Pooled data from n=3 experiments. **(G)** Quantification of global protein production by incorporation of O-propargyl-puromycin (OPP) into nascent peptides (n=6). Paired t-test between untreated and cycloheximide groups. Two-way ANOVA with Dunnett's post hoc test between all siRNA treated groups. ns indicates not significant. $*p \leq 0.05$, $****p \leq 0.0001$.

Figure 5

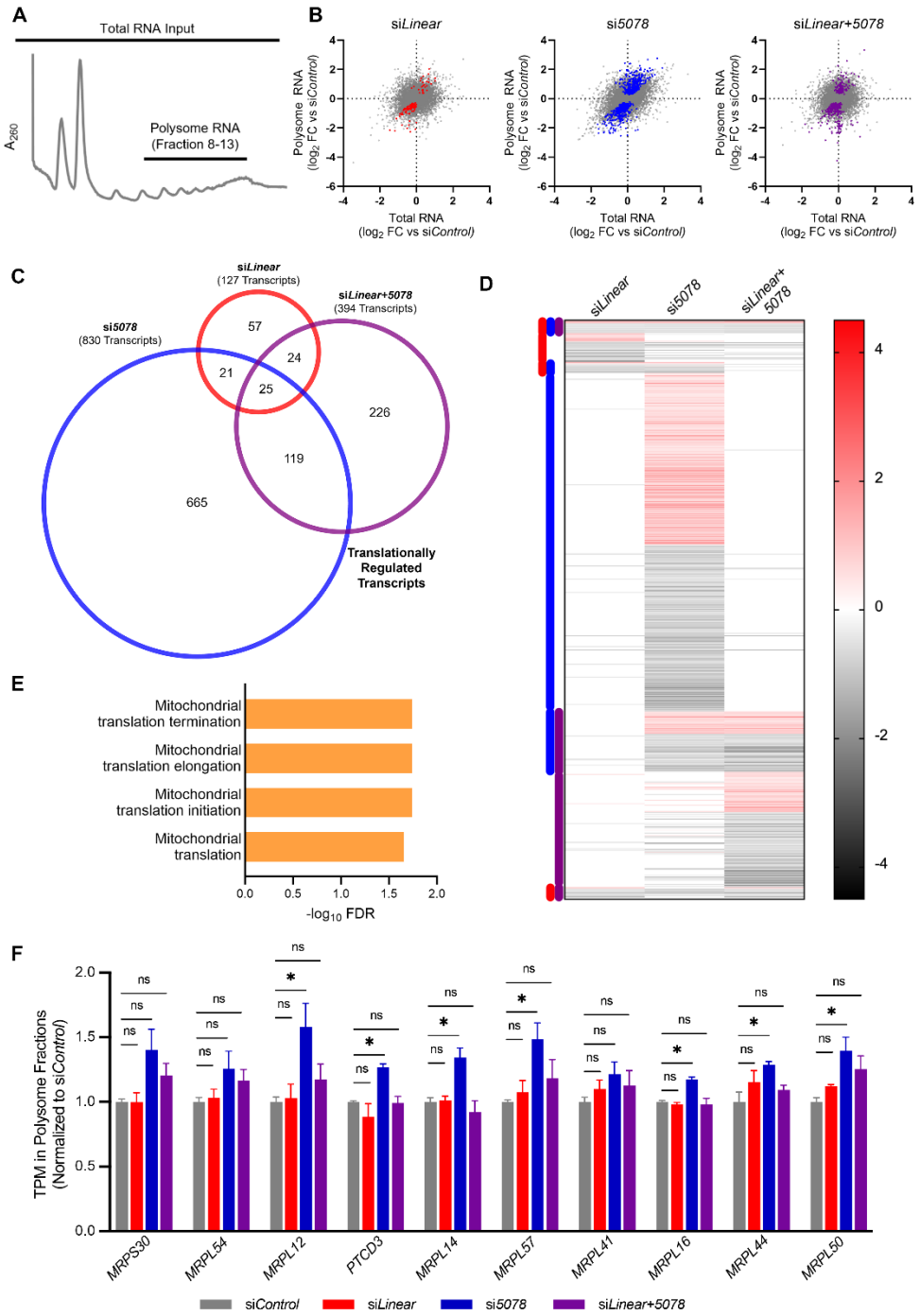

Figure 5. Loss of *circ5078* in HPAECs induces increased translation of nuclear encoded mitochondrial ribosome components. (A) RNA sequencing was performed on total input RNA from unfractionated lysates, and RNA from the actively translated Fractions (8-13) of polysome profiles for HPAECs treated with si*Control*, si*Linear*, si*5078*, or si*Linear+5078* siRNAs. n=3 independent experiments. **(B)** Scatter plots of the $\log_2$ fold change versus si*Control* in both total

RNA and polysome RNA fractions for each siRNA condition. Highlighted transcripts are those deemed to be translationally regulated ($p_{adj} \geq 0.05$ in input fraction, $p_{adj} < 0.05$ in polysome fraction). **(C)** Venn diagram and **(D)** heatmap of genes regulated by translation in at least one of the three conditions. **(E)** Summary of pathways enriched among the transcripts in which translation was upregulated by *circ5078* loss alone, as identified by Reactome. **(F)** Relative expression in polysome fractions of transcripts encoding components of the mitochondrial translation pathway. One-way ANOVA with Dunnett's post hoc test for each transcript. ns indicates not significant. *$p \leq 0.05$.

Figure 6

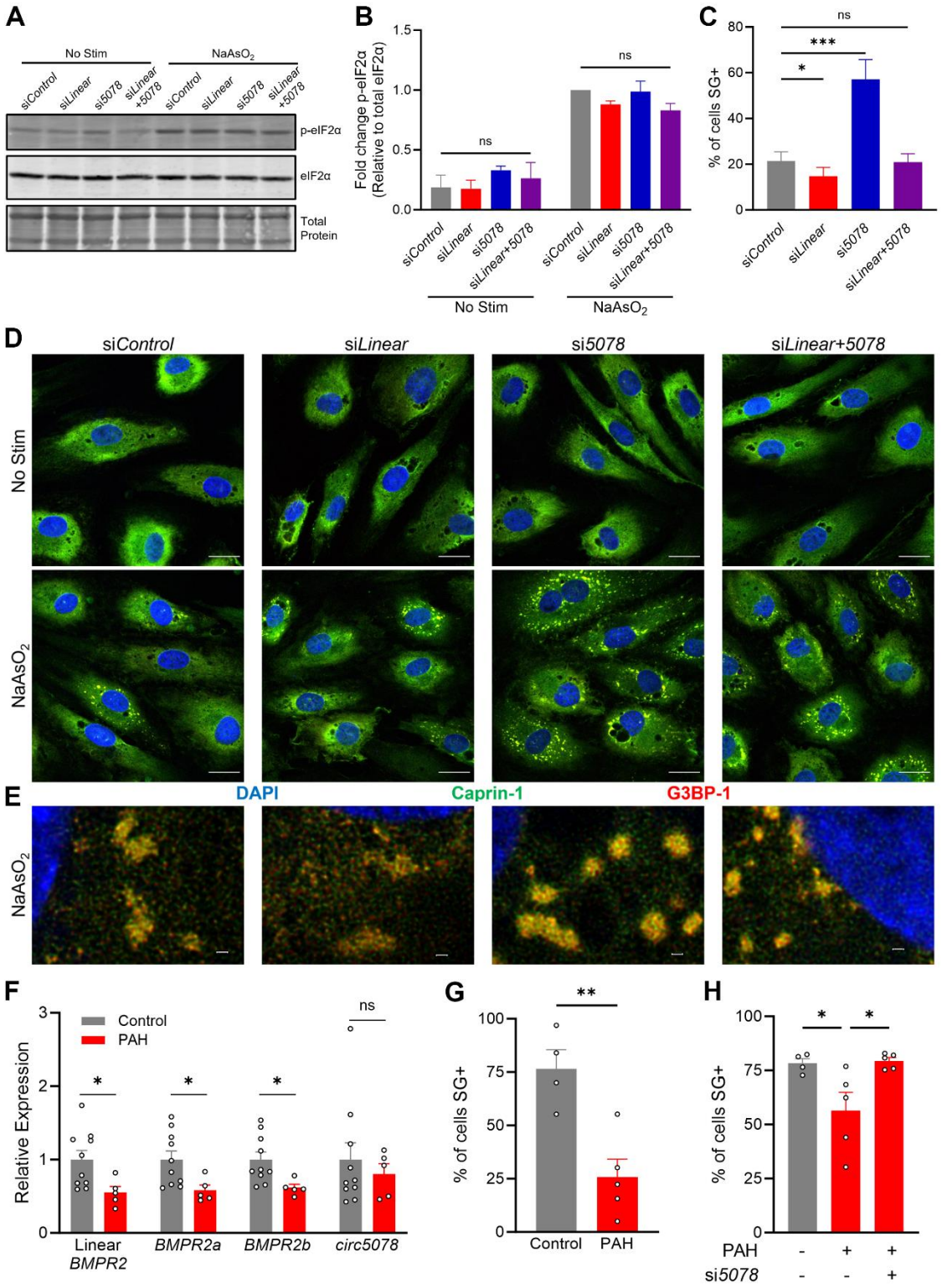

Figure 6. Linear and circular *BMPR2* transcripts differentially modulate Caprin-1 granule formation. (A) Representative immunoblot and **(B)** quantification of phosphorylated eIF2α in

HPAECs treated with si*Control* (grey), si*Linear* (red), si*5078* (blue), or si*Linear+5078* (purple) siRNAs, with or without treatment with 100 μM sodium arsenite for 1 hour (n=3). **(C)** Quantification (n=9), and **(D)** representative confocal (Scale bar = 20 μm), and **(E)** STED super-resolution (Scale bar = 0.5 μm) images of stress granules in cells stained with Caprin-1 (green) and the stress granule marker G3BP-1 (red) under each condition. **(F)** Relative expression of linear *BMPR2*, *BMPR2a*, *BMPR2b*, and *circ5078* transcripts in blood outgrowth endothelial cells from *BMPR2* mutation-bearing PAH patients (n=5) and healthy controls (n=10). **(G)** Quantification of cells with stress granules in BOECs from healthy controls (n=4) and PAH patients (n=5) in response to sodium arsenite. **(H)** Stress granule production in control BOECs treated with si*Control* (n=4), and PAH BOECs treated with si*Control* or si*5078* (n=5). **(B, C and H)** One-way ANOVA with Dunnett's post hoc test. **(F, G)** Unpaired t-test. ns indicates not significant. $*p \leq 0.05$, $**p < 0.01$, $***p < 0.001$.